Spectral dependence of carrier lifetimes in silicon for photovoltaic applications

John F. Roller,[1] Yu-Tai Li,[2] Mario Dagenais,[3] and Behrang H. Hamadani[1]
[1]*Engineering Laboratory, National Institute of Standards and Technology, Gaithersburg, Maryland 20899, USA*
[2]*PV Metrology Laboratory, Industrial Technology Research Institute, Chutung, Hsinchu 31040, Taiwan*
[3]*Department of Electrical and Computer Engineering, University of Maryland, College Park, Maryland 20742, USA*

(Received 24 August 2016; accepted 5 December 2016; published online 21 December 2016)

Charge carrier lifetimes in photovoltaic-grade silicon wafers were measured by a spectral-dependent, quasi-steady-state photoconductance technique. Narrow bandwidth light emitting diodes were used to excite excess charge carriers within the material, and the effective lifetimes of these carriers were measured as a function of wavelength and intensity. The dependence of the effective lifetime on the excitation wavelength was then analyzed within the context of an analytical model relating effective lifetime to the bulk lifetime and surface recombination velocity of the material. The agreement between the model and the experimental data provides validation for this technique to be used at various stages of the solar cell production line to investigate the quality of the passivation layers and the bulk properties of the material. [http://dx.doi.org/10.1063/1.4972409]

I. INTRODUCTION

Measurement of the charge carrier lifetimes in photovoltaic (PV) materials has become a routine diagnostic practice for evaluating the material quality, oftentimes early in the manufacturing process. In fact, it has been shown that a longer lifetime generally correlates with a higher solar cell efficiency.[1,2] In thin semiconductor wafers where the intrinsic charge carrier lifetimes are long enough so that the corresponding diffusion length of charge carriers is on the order of the material thickness or smaller, the surface effects can play a dominant role on the measured *effective* charge carrier lifetime.[3–7] When the surfaces of a wafer are not properly passivated,[7] the surface recombination velocity, S, can be very high. Under these conditions, a very high-quality, high-bulk-lifetime material will show significantly lower effective lifetimes, therefore masking the properties of the bulk.

For photovoltaic (PV) applications, Si, particularly in single-crystalline and multi-crystalline wafer form, is still the most widely-used material for industry; therefore, understanding the material properties including bulk lifetimes and the quality of the surface passivation is a top priority for many PV module manufacturers.[8,9] In order to separate bulk from surface effects, several approaches and techniques have been previously developed.[3–5,10–20] The most common approach involves the contactless photoconductance (PC)-based quasi-steady-state (QSS) measurements[8,21,22] and modeling of the effective lifetime on a large set of wafers with varying degrees of processing[9] or wafers with arbitrary thicknesses but otherwise of similar surface passivation processes.[10] However, access to a large set of wafers for such types of analyses may not be always possible or convenient. In addition to the steady state or the QSS photoconductance approach, optical transient decay experiments[5,16–18,23–25] have also been used, mostly consisting of pump-probe or two-beam measurement techniques. Surface vs. bulk effects can be determined by examining the temporal behavior of the decaying probe signal. In addition to this method, microwave photoconductivity decay has also been used to characterize wafers. This process involves measuring the reflected power of incident microwaves, which is proportional to excess charge carrier concentration.[3,13,18,25,26] These techniques generally require an extensive and costly experimental setup, and are not widely used in a manufacturing setting.

In this work, we investigate the spectral dependence of the effective lifetime within the context of a recently-developed analytical model[10] to explore what types of information regarding the bulk and the surface effects can be extracted from the wavelength-dependent measurements. This spectral dependence is, to some degree, the result of the wavelength dependence of the absorption coefficient of light in the material, and is most pronounced when surface effects are dominant over bulk properties. We used an array of monochromatic light emitting diodes (LEDs) with a wide range of wavelengths coupled with a contactless radio frequency (RF) photoconductance measurement apparatus to determine the lifetimes of a set of passivated and unpassivated Si wafers as a function of wavelength and intensity. Specifically, our work was focused on the QSSPC method, which is a very well-established technique and made it possible to take advantage of the steady-state equations of charge carrier transport developed in Reference 10. The plurality of the spectral dependence studies in the literature has been achieved with transient methods employing tunable fast laser pulses and time resolved detection.[4,5,16–18,20] The few reports of spectral-dependent effects to-date, utilizing the QSSPC method and governing equations, have been mostly focused on the use of bandpass filters to select a given spectrum from a broad-spectrum flash source.[11,12,14,15] LEDs are more advantageous in such measurements because they are relatively easy to operate and the temporal profile of the light can be electronically controlled by using simple equipment such as a waveform generator. Intensity can also be precisely controlled by the magnitude

of the sourced current in addition to filters. Furthermore, scaling up intensity is easily achievable by mounting a large number of LED chips on a metal-clad printed circuit board to increase the overall light output and achieve a better signal-to-noise ratio for low PC signals. More significantly, we were able to trigger our LEDs to apply tens or hundreds of QSS signal pulses to the wafer under test and average the resulted PC signal so that a better signal-to-noise ratio can be achieved even under very low intensities. Use of a selected few LEDs to make lifetime measurements have been reported, albeit without providing any analysis of any spectral effects.[27]

Several samples were measured using this photoconductance measurement technique and the data were found to fit the spectral-dependent model relatively well. Spectral dependence of the effective lifetime is most apparent with unpassivated or poorly passivated silicon wafers where the surface recombination velocity is not low. The surface recombination velocities, in these cases, can be reliably extracted using the model. However, the exact value of the bulk lifetime cannot be always extracted from the model, as the sensitivity of the model to the bulk lifetime parameter is dependent upon the wafer thickness and also to the extent of the domination of surface effects. We will discuss these issues in detail in this work. Although our focus is on PV applications, it should be noted that this technique can be used for other applications in the semiconductor industry, the molecular electronics field, or nanotechnology where the knowledge of bulk lifetimes or the passivation state of wafers (silicon or non-silicon materials) may be needed.

II. EXPERIMENTAL DETAILS

For these measurements, the Sinton WCT120 instrument (see disclaimer) was modified so that the photoconductance measurement coil and circuitry can be triggered by an LED array light source instead of the default broadband flashlamp source. Nine high-powered LEDs were selected in the wavelength range from 456 nm to 1032 nm, and custom-electronics were designed and fabricated to control their output flux and their temporal irradiance profile so that the QSS conditions can be met for a wide range of carrier lifetimes, including effective lifetimes approaching 1 ms.

The LEDs were operated in a periodic sinusoidal functional form, with the timing of the waveform synchronized with the photoconductance signal collection. This task was achieved by use of a function generator and a custom power amplifier that allows for any input light profile, including the sinusoidal waveform used here. Operation of the LEDs in waveform, particularly for very short effective lifetime materials, allowed us to measure the PC signal over tens or hundreds of waveform periods, resulting in improved signal-to-noise ratios even under very low charge carrier densities. For example, by using this method, effective unpassivated wafer lifetimes as short as 30 ns were measured at an excess carrier density as low as $\approx 10^{12}\,\mathrm{cm}^{-3}$. By changing the input frequency on the function generator, we were able to control the temporal profile of the light output and hence the PC signal. This approach allowed us to perform the QSS measurement on wafers with very long lifetimes at a variety of unique wavelengths. For the initial measurements, the input signal used was a sine wave with a frequency of 9.7 Hz. Most of the measurements were taken with a slower frequency of 0.97 Hz. The ability to change this frequency helped when transient effects became apparent for some long lifetime materials.

The measurement schematics and a photo of the modified system are shown in Figs. 1 and 2. The light output of the LEDs is coupled into a polished quartz light pipe to capture as many photons as possible and deliver a uniform light intensity to the wafer location over the entire area of the coil. The quartz light pipe is suspended over the sample by the 3-d printed black mount seen in Fig. 2. Figure 3 shows the normalized spectral irradiance of all the LEDs used for these measurements, along with the calculated center wavelengths for each LED. This plate was mounted on a water-cooled stage fed by a circulator bath with a setpoint temperature of 15 °C to keep the LEDs thermally stable. The intensity of the illumination can also be controlled by the magnitude of the current sourced through the LEDs. The LED intensities at the illumination/measurement plane were generally in the range of 10 $\mathrm{W/m^2}$ to 1000 $\mathrm{W/m^2}$, comparable to the normal operating exposure of actual installed solar modules.

A computer code was developed to facilitate the triggering, acquisition, and analysis of the data. In addition to PC signal measurements, LED light intensity measurements were also performed as a second measurement at the irradiance plane of the sample. This measurement was achieved by use of a calibrated reference photodiode in irradiance spectral response mode. Furthermore, the spectral irradiance of each of the 9 LEDs was also measured separately (see Fig. 3) by a spectroradiometer and used in the calculation of the generation rate as explained later. Finally, reflectance measurements were performed on each wafer using a technique involving a monochromator and an integrating sphere

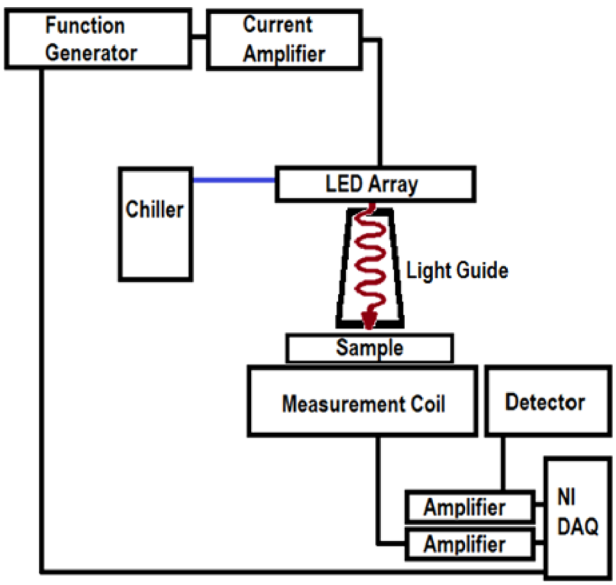

FIG. 1. Schematic of the photoconductance lifetime measurement system. The LED array driving the lifetime measurement is run by a function generator coupled with a power amplifier and temperature controlled by a water chiller. The measurement is done through a data acquisition system attached to a measurement coil and detector.

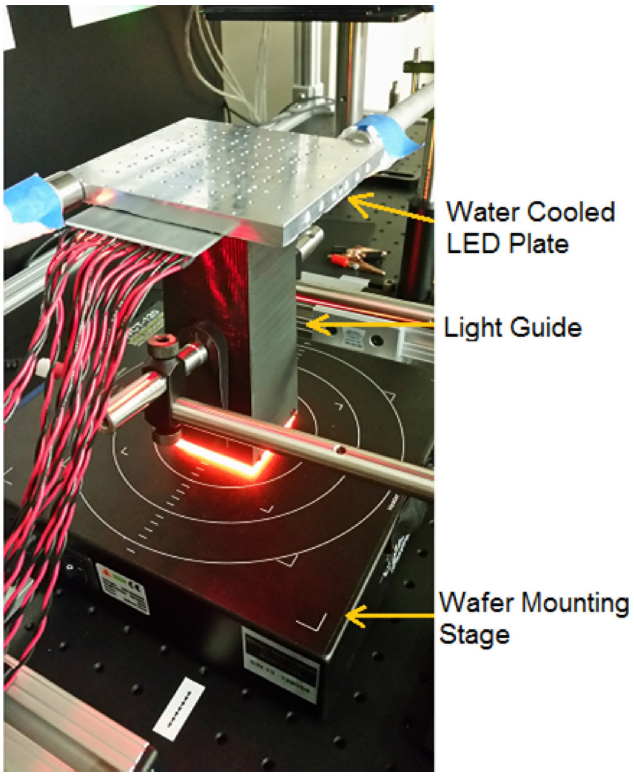

FIG. 2. Measurement setup using the Sinton WCT120 base and the water cooled LED array with the light guide. The light guide is made from quartz and encased with a 3D printed holder. Note the uniform output of the LED array on the stage.

so that optical losses due to reflection mainly off the front surface can be incorporated into the generation rate calculations.

Although the light pipe provides a reasonably good irradiance uniformity at the sample plane, there is still room for improvement. For these measurements, depending on the location of the mounted LED and its coupling into the light pipe, non-Gaussian irradiance nonuniformity of around 7% to 11% over the illuminated area of about 50 mm × 50 mm was observed. A small aperture photodetector was used to map the irradiance plane. In addition to the effect of nonuniformity, the photoconductance signal also shows a range of

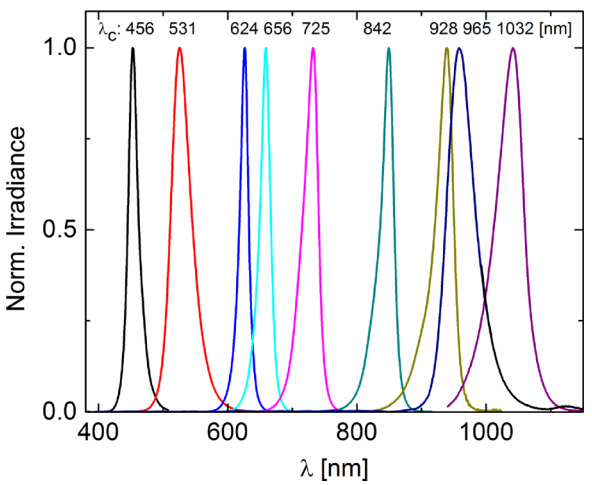

FIG. 3. Normalized spectral irradiance of the 9 different high-powered LEDs used for these experiments.

statistical variations depending on the signal level. For each type of material that was measured, we performed a series of measurements with one representative LED to evaluate the effect of these variations. The standard deviations of this uncertainty analysis are added to the data plots discussed later and range anywhere from 5% to 33% of the mean value.

III. METHODOLOGY

A. Calculation of effective lifetimes

The measurements of the effective lifetimes, τ_{eff}, are based on the continuity equation for the excess carriers, Δn, and in the most generalized form, for both the QSS and the transient measurements, can be expressed as[22]

$$\tau_{eff} = \frac{\Delta n}{g - \frac{d\Delta n}{dt}}, \tag{1}$$

where g is the generation rate. Under steady state conditions, the transient term $d\Delta n/dt$ is negligible, and hence the effective lifetime of a sample can be obtained by determining the number of charge carriers and the generation rate in the material.

Δn is related to the photoconductance $\Delta\sigma$ generated in the material under illumination, and it was determined for all the measurements as outlined in the literature.[21,28] Here, we explain the determination of the total generation rate g:

First, the incident photon flux ϕ for each LED is determined

$$\phi(\lambda) = \frac{\hat{E}_{e,\lambda} V}{R(\lambda) G} \frac{\lambda}{hc}. \tag{2}$$

The photon flux, measured in photons per second per unit area, is a function of the normalized spectral irradiance of the LED, $\hat{E}_{e,\lambda}$, the voltage measured by the photodetector, V, the responsivity of the detector, $R(\lambda)$, the gain of the transimpedance amplifier connected to the photodetector, G, the wavelength, λ, Planck's constant, h, and the speed of light, c. An integration was performed over the actual irradiance curve to calculate the integrated intensity for the LED. The actual irradiance was then scaled by the integrated intensity in order to get the normalized spectral irradiance curve, $\hat{E}_{e,\lambda}$. With the absorption coefficient α of Si obtained from tabulated results[29] and the spectral reflectance measurements $r(\lambda)$ as described above, the total generation rate g can be determined

$$g = \int_0^w \int_{\lambda_{min}}^{\lambda_{max}} \alpha(\lambda) \frac{\hat{E}_{e,\lambda} V}{R(\lambda) G} \frac{\lambda}{hc} e^{-\alpha(\lambda) z} (1 - r(\lambda)) d\lambda \, dz, \tag{3}$$

where integrals are performed over the depth dimension z up to the wafer thickness w and over the lower and upper wavelength bounds for the LED spectrum. This equation assumes that reflection losses occur mainly at the front surface of the wafer and is mostly valid for wavelengths up to 900 nm. For higher λ and particularly textured wafer surfaces, a path-length enhancement factor is considered.[30] Furthermore, the use of the light pipe for light delivery results in a certain distribution of non-normal angles of incidence of light, the

exact nature of which depends on the LED light coupling into the pipe, the LED angle of emission, etc. A mismatch between the cosine response of the reference photodetector and the wafers can also affect the calculation of the generation rate. For wavelengths in the range of 400 nm to 900 nm, the absorption depth of the radiation is much smaller than the wafer thickness of even our thinnest wafers. Therefore, the light absorption and carrier generation is likely unaffected by non-normal angles. We have verified this by comparing the light pipe measurements of the lifetimes with either the Sinton light source or separate collimated LED light measurements. For the LEDs in the range of 900 nm to 1200 nm, the absorption depth starts to become comparable to the thickness and therefore the generation rate in the wafer can get affected by how far the light penetrates before it is either absorbed or it reaches the bottom interface resulting in a reflection or transmission. This effect could be a source of error, although the exact amount requires further investigation.

B. Comparison of the LED method with current measurement techniques

The LED-based measurement was partly validated by comparison to a similar measurement performed with the calibrated Sinton WCT-120 system. The comparison between the two methods can be seen in Fig. 4, where the τ_{eff} measured by both a 725 nm LED and the WCT-120 flashlamp is plotted as a function of the excess carrier density for a silicon nitride-passivated n-type reference Si wafer. The WCT-120 measurement program calculates the lifetimes with inputs of the thickness of the wafer, resistivity, sample type, and an optical constant. This optical constant is an estimated value based on the optical models and accounts for reflectance and transmittance effects. Although the LED-based measurement cannot generate as high of an excess carrier density as the commercial system does, the agreement is reasonable over the carrier density range probed. We also verified that this agreement holds for other LEDs and a few other passivated wafers.

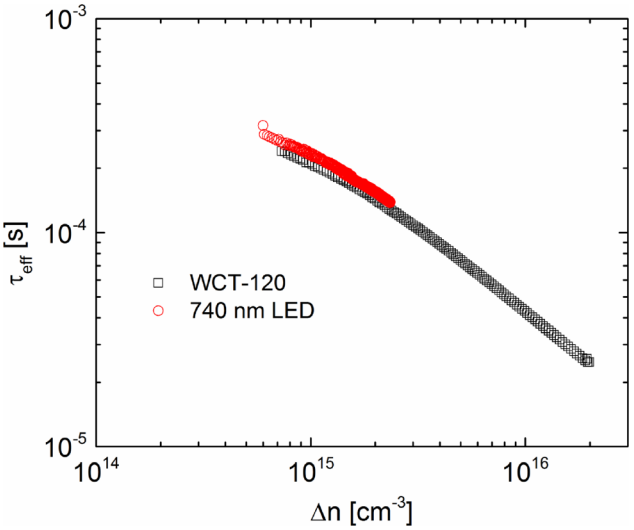

FIG. 4. Comparison of lifetime data between the LED measurement system and the Sinton WCT-120 instrument.

C. Effect of traps

It has been shown that the trap states can lead to a relatively large photoconductive response at relatively low input light intensities.[31–34] This effect, when left unaccounted for, causes the measured photoconductivity to be artificially high and therefore the lifetime calculation would result in an incorrect value (also artificially high). The excess carrier lifetimes in such cases can be accounted for by using a bias term that subtracts out the photoconductive effects of the traps.[32] Although it is generally common to see the effects of traps in polycrystalline Si materials, monocrystalline silicon wafers, particularly with unpassivated surfaces, can also reveal trap-related effects.

Figure 5 shows a plot of Δn vs. g for an unpassivated Si wafer lifetime measurement with the 725 nm LED. At generation rates below $\approx 10^{17}\ \mathrm{cm^{-3}\,s^{-1}}$, the photoconductance signal is dominated by traps, therefore the actual recombination lifetime should be calculated based on the change of Δn with respect to g above a threshold generation rate, or as the slope of a fit to the curve above $g = 10^{17}\ \mathrm{cm^{-3}\,s^{-1}}$ for this case. It should be noted that this approach can be applied to all samples, but is especially important for the unpassivated wafers measured in this study. This importance is due to the high trap concentration and low photoconductive response in these materials, particularly near the surfaces. Passivated samples such as the reference sample also show photoconductive trap effects, but they are minimal by comparison to the overall photoconductive signal generated.

IV. DISCUSSION AND RESULTS

A. Numerical modeling

Before we discuss the results of the spectral-dependent measurements and the analytical model, we present the outcome of several numerical calculations based on drift-diffusion equations. These calculations explain the effects of wavelength and the surface recombination velocity on excess carrier density, plotted as a function of the wafer depth. This modeling serves to demonstrate multiple points. First, it can

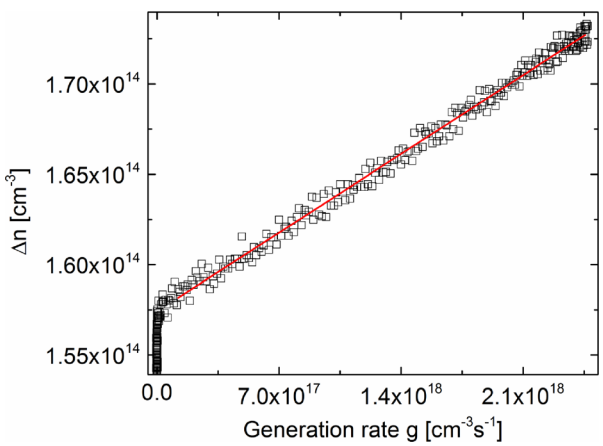

FIG. 5. Excess Carrier Density vs. Generation Rate curve for the 1 mm Si wafer with a 725-nm LED input. The effective lifetime is calculated using the trendline through the measured data points. The equation for the trendline is given by $\Delta n = 6.56 \times 10^{-6}\, g + 1.18 \times 10^{14}\ \mathrm{cm^{-3}}$ giving an effective lifetime of $\tau_{eff} = 6.56\,\mu\mathrm{s}$.

be used to determine a representative carrier density and effective width of the material such that there will be one value for Δn generated within the wafer. This determination is particularly important for thick wafers where Δn shows a strong depth dependence. Second, the modeling based on one shorter and one longer wavelength reveals the distribution of the excess carrier density within the z dimension under the influence of weak and strong surface effects. Finally, the results demonstrate why τ_{eff} has a spectral dependence that is most pronounced at higher surface recombination velocity values.

The generation rate varies as a function of depth within a material, with more photons absorbed near the front surface of the wafer than deeper within the wafer due to absorption and transmission effects. The photogenerated electrons and holes will diffuse through the material and reach the steady-state equilibrium. For thick wafers, the effective excess charge carriers, Δn_{eff}, will only be represented within an effective width, w_{eff}, outside of which the model assumes an excess carrier density of 0. Δn_{eff} and w_{eff} are defined in Equations (4) and (5), respectively[35,36]

$$\Delta n_{eff} = \frac{\int_0^w \Delta n^2 dz}{\int_0^w \Delta n\, dz}, \tag{4}$$

$$w_{eff} = \frac{\left(\int_0^w \Delta n\, dz\right)^2}{\int_0^w \Delta n^2 dz}. \tag{5}$$

Since the wafer is assumed to be in the quasi-steady-state, all temporal effects can be neglected. Also, the wafer is not subject to an external field so the drift current is negligible. This simplification reduces the diffusion equation in one dimension to Equation (6), where the density of charge carriers, say, n for electrons, and the generation rate, g, are both functions of depth, z

$$D\frac{d^2n(z)}{dz^2} - \frac{n(z)}{\tau_b} = -g(z). \tag{6}$$

Here, D is the ambipolar diffusion constant of charge carriers.[10] In order to numerically solve this model, a mesh of points is constructed evenly spaced in z, and boundary conditions based on the surface effects are added. These boundary conditions are shown in Equations (7) and (8) where S is assumed to be the same for both the front and back surfaces[4,5,11]

$$D\frac{dn(z)}{dz}_{z=0} = S\,n(0), \tag{7}$$

$$-D\frac{dn(z)}{dz}_{z=w} = S\,n(w). \tag{8}$$

Figures 6(a)–6(d) show several runs of the numerical model with varying conditions for the incident LED illumination wavelength λ, and the surface recombination velocity, S. For the purpose of meaningful comparison, the numerical simulations are performed in such a way that the total generation rate for each case is the same. In Figs. 6(a) and 6(b), S is kept fixed at a low value of 2 cm/s and only λ is changed from 531 nm to 928 nm, corresponding to the center emission

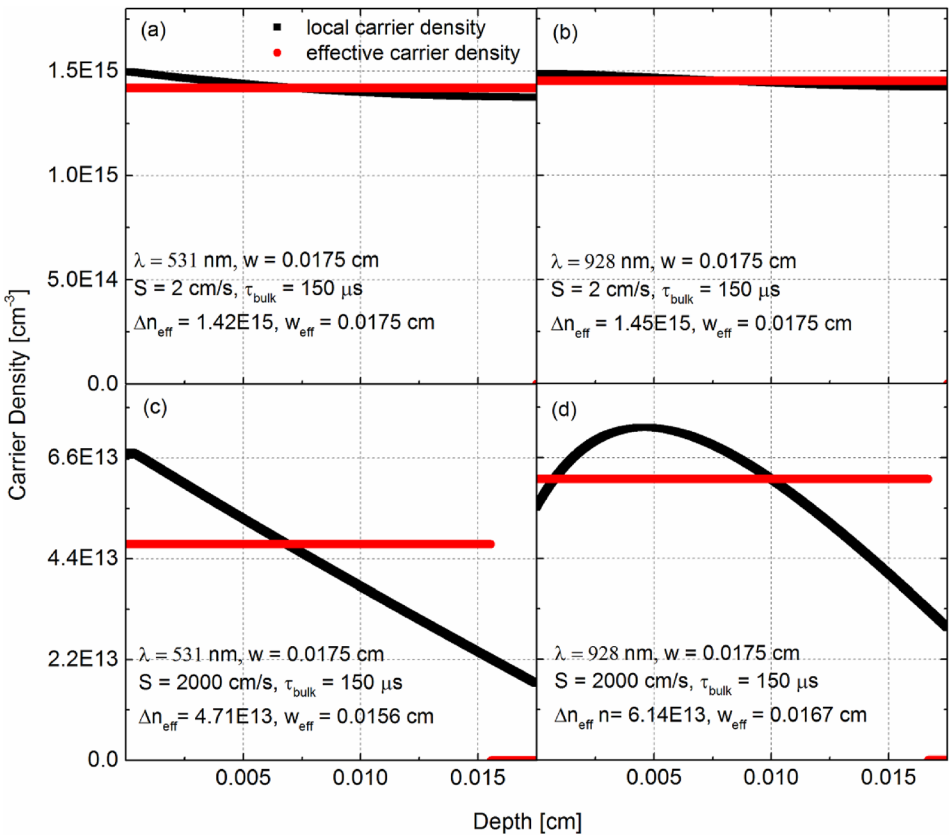

FIG. 6. Simulations of depth dependence of excess carriers in a silicon wafer. Two input spectra corresponding to LEDs with effective wavelengths of 531 nm and 928 nm were used to calculate the steady state responses shown. The assumed S values are similar to those extracted from some of the wafers measured and discussed. The simulation parameters and results are shown for each case.

wavelengths of two of our LEDs. Also, w is chosen corresponding to the thickness of typical solar cell grade wafers that we received from the manufacturer. Note how the local carrier density is relatively constant throughout the z dimension and is also very close to the effective carrier density. Furthermore, the calculated Δn_{eff} between the two cases are very similar, with the small difference mostly due to the mesh size chosen for the calculation (so that the calculation can be done in a reasonable time frame). With g kept the same for both cases, one can see that $\tau_{eff} = \Delta n_{eff}/g$ remains unchanged between the two cases, even with the substantial difference between the absorption and generation profile of these two conditions.

Figs. 6(c) and 6(d) show a similar calculation with the sole difference that S has been increased to 2000 cm/s. In this case, a considerable change can be observed in the carrier density profile throughout the bulk when λ is changed from 531 nm to 928 nm. Since the 928 nm LED generates more carriers in the bulk than the green LED (mostly absorbed near the surface), the distribution of carriers away from the incident interface ($z = 0$) remains high and in fact is more than the front surface where the surface recombination effects reduce the local carrier density. This effect causes the Δn_{eff} for the 928 nm LED to be higher than the 531 nm LED, therefore resulting in a $\approx 30\%$ increase in the effective charge carrier lifetime. Finally, note that the effective wafer thicknesses are lower than the modeled wafer thicknesses for these two cases. Therefore, it can be shown that the spectral effects in materials with high surface recombination velocities can influence the measurement of the effective lifetimes. Conversely, measurements of lifetimes as a function of illumination wavelength show a spectral dependence at high S that under the right circumstances can be used to separate the bulk lifetime and the surface recombination velocity. This task is most readily achieved through an analytical model derived from the same equations discussed here.

B. Analytical model of the spectral dependence of lifetime

The numerical observations that were discussed in Section IV A were recently explored by Turek and coworkers[10,37] and were placed within an analytical framework that can better establish the connection between the modeled parameters. Using the same base diffusion differential equation (6), a solution is found in the form of

$$n(z) = c_1 e^{\frac{z}{l}} + c_2 e^{-\frac{z}{l}} + c_3 e^{\alpha z} + c_4 e^{-\alpha z}. \tag{9}$$

The parameter l in this equation is the charge carrier diffusion length and is defined as $l \equiv \sqrt{\tau_b D}$ where τ_b is the bulk lifetime of the material. The boundary conditions given in Equations (7) and (8) can be used to find the coefficients c_{1-4}. Equation (9) with determined coefficients and a generation rate equation given by Equation (10) are then used to calculate an effective lifetime according to Equation (11). In the generation rate equation, P_λ is the illumination power, A is the wafer area, and r is the reflection coefficient

$$g_\lambda(z) = \frac{\lambda P_\lambda}{Ahc}(1-r)\alpha e^{-\alpha z}, \tag{10}$$

$$\tau_{eff} = \frac{\int_0^W n(z)dz}{\int_0^W g_\lambda(z)dz}. \tag{11}$$

The analytical solution to Equation (11) is found to be the wavelength-dependent relation

$$\tau_{eff,\lambda} = \frac{\tau_b}{1-\alpha^2 l^2}\left[1 - \alpha l \frac{\alpha l + \frac{Sl}{D}\coth\frac{\alpha w}{2}}{1 + \frac{Sl}{D}\coth\frac{w}{2l}}\right]. \tag{12}$$

This analytical solution shows that the effective lifetime at a specified wavelength, $\tau_{eff,\lambda}$, is a function of the bulk lifetime of the material, τ_b, the wavelength dependent absorption coefficient, α, the surface recombination velocity, S, the total width, w, the diffusion length, l, and the diffusion constant, D. Before we describe how Eq. (12) can be used to model the spectral dependence of charge carrier lifetimes in several types of silicon wafers, it will be helpful to first explore what exactly Eq. (12) predicts and how sensitive the parameters τ_b and S are to changes in τ_{eff} with wavelength.

C. Sensitivity range for the analytical model

There are certain issues that need to be considered when using Eq. (12) to explain the experimental results. In general, a higher surface recombination velocity results in more pronounced spectral effects. Therefore, the spectral dependence of τ_{eff} can generally be used to extract S for unpassivated or poorly passivated wafers. Figures 7(a)–7(c) show the modeled behavior of τ_{eff} vs. λ for a n-type silicon wafer with $w = 160\,\mu$m and Figures 7(d)–7(f) show the same behavior for a much thicker wafer with $w = 5$ mm. For both the thin and thick wafers, it can be seen that the spectral dependence of τ_{eff} only appears when S is around a few hundred cm/s and becomes more substantial as S increases. However, for a fixed S, as τ_b increases, the effective lifetime behavior approaches a limiting case and will not change further. For thin wafers, this limiting behavior occurs at lower bulk lifetimes for larger S. For example, Fig. 7(a) shows that for $S = 10^5$ cm/s, all the curves with $\tau_b \geq 100\,\mu$s collapse onto one curve, whereas for $S = 10^3$ cm/s, this limiting behavior occurs at $\tau_b \geq 1$ ms. This insensitivity of the model to cases of higher bulk lifetimes at higher surface recombination velocities limit one's ability to precisely extract *both* these values from the fit of the experimental data to the model because τ_b loses its uniqueness. In such cases, the value of S is the only parameter that can be determined reliably and only a lower bound for τ_b may be given. One way around this limitation is to obtain thicker wafers of similar bulk and surface properties and perform the spectral dependent measurements on them. As Fig. 7(d) demonstrates, at $w = 5$ mm, the bulk lifetime sensitivity extends to at least 10 ms, which will allow for determination of both parameters, up to this bulk lifetime, at the same time. Understanding

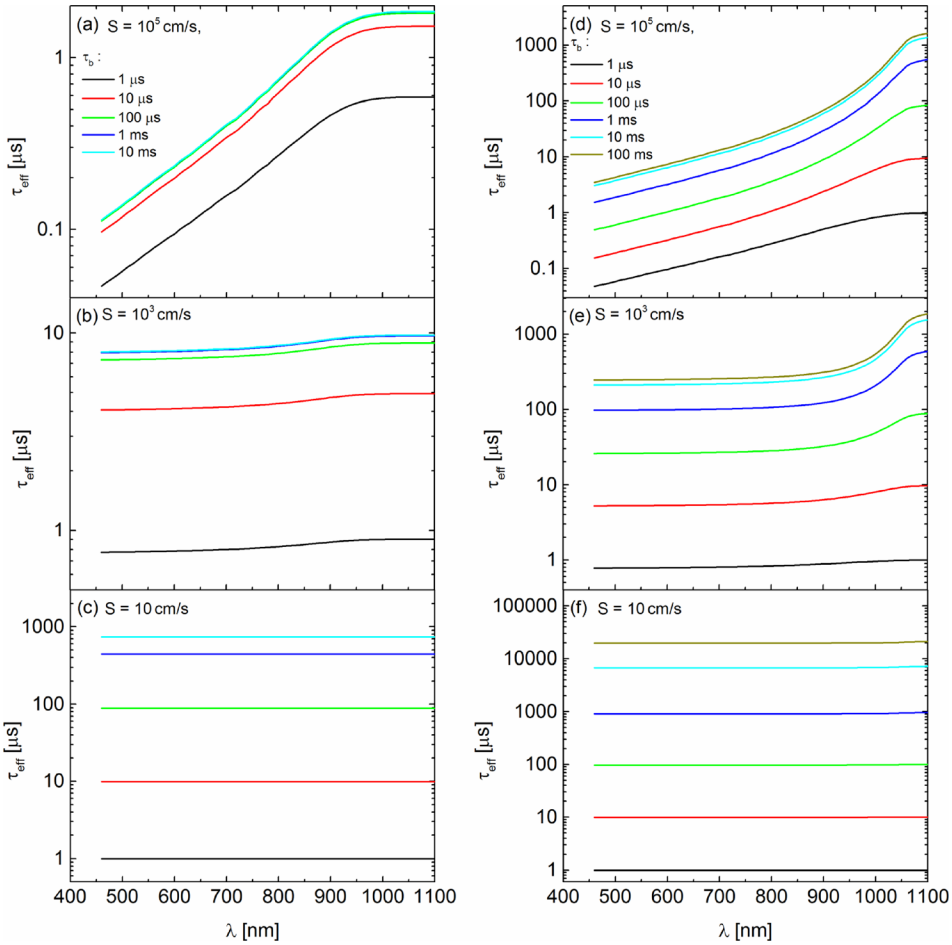

FIG. 7. ((a)–(c)) Modeled behavior of τ_{eff} vs. λ for a n-type silicon wafer with $w = 160\,\mu$m and 3 sets of S values. ((d)–(f)) The same behavior for a wafer with $w = 5$ mm. The diffusion coefficient of holes, $D = 12\,cm^2/s$, was used in these calculations.

these limitations is important prior to any modeling work on the measurement results. When fitting the model to the data, the uniqueness of the fit parameters, particularly τ_b, should be verified over a large range of values in order to validate the convergence of the fit parameters. Section IV D describes some experimental findings.

D. Agreement between the model and the experimental results

The validity of the model described in Section IV B was explored by comparing the model predictions with the experimental data obtained from four sets of wafers. The first type was a 550 μm-thick, n-type polished silicon wafer with an intrinsic bulk resistivity of 0.34 Ω cm without any surface passivation. The second wafer was a 1-mm-thick, double-side polished n-type Si wafer with no surface passivation and an intrinsic bulk resistivity of 10 Ω cm. The third type consisted of two surface-textured n-type 160 μm-thick wafers from a PV manufacturing plant (resistivity ≈ 3.5 Ω cm), one wafer without any passivation process (hence called *unpassivated*) and another processed by deposition of an amorphous intrinsic silicon layer (≈5 nm to 10 nm) on both sides, followed by a doped amorphous p+ silicon layer (≈5 nm to 10 nm) on one side and an amorphous n+ silicon layer (≈10 nm to 20 nm) on the other side (referred to here as *passivated*, although it does contain the emitter layer too). Finally, the fourth wafer type consisted of two surface-textured wafers that are p-type of thickness 175 μm (resistivity ≈ 1.6 Ω cm), one cleaned but unpassivated and the other having gone through the process of emitter layer deposition on one face and passivation layer deposition on the other. The n-type wafers were obtained from a manufacturing line of Heterojunction with Intrinsic Thin-layer (HIT) solar cells, and the p-type wafers were provided by a manufacturer of Passivated Emitter Rear Contact (PERC) solar cells.

Figure 8(a) shows the experimental results and the analytical model fit to the data for the 550 μm thick wafer. From the best fit of the model to the data, $\tau_b = 63\,\mu$s and $S = 8800$ cm/s were extracted at an excess carrier density of $\approx 10^{13}\,cm^{-3}$. We found that the model converges well for these two values, consistent with the sensitivity analysis presented earlier. In this case, the spectral dependent measurements have successfully been used to separate the bulk lifetime from the surface recombination velocity. Here, parameter $D = 12\,cm^2/s$ and $\alpha(\lambda)$ values were chosen and kept fixed based on the accepted literature results.[29] Figure 8(b) however shows the measurement results and the analytical model fit to the data for the 1 mm-thick wafer. In this case, although the model fits well to the data and there is good confidence over the extracted $S = 10\,600$ cm/s, we observe that we can only state a lower bound value of $\tau_b \geq 2$ ms for the bulk lifetime because the data is beyond the sensitivity range of the model. In fact, recent results suggest that the bulk lifetimes for such high resistivity wafers can be as high as 30 ms.[38] Therefore, it can be seen from these two

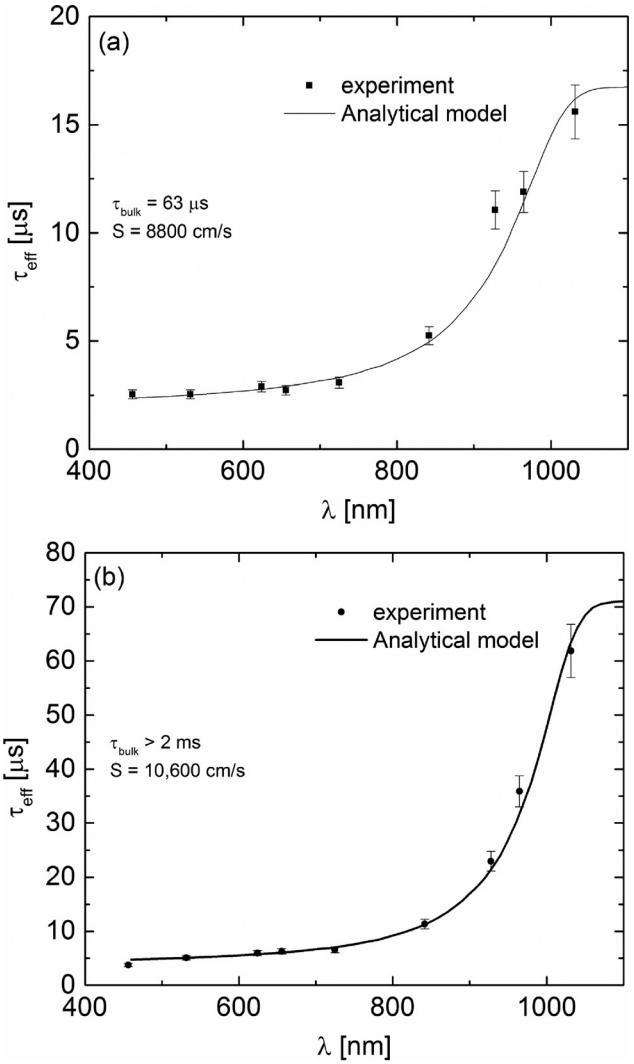

FIG. 8. (a) Measured data and the analytical model fit for the 0.55-mm n-type unpassivated wafer. The analytical model was fit with values of $\tau_b = 63\ \mu s$ and $S = 8800$ cm/s and $D = 12\ cm^2/s$. (b) The experimental results and the analytical model fit for the 1 mm thick, high resistivity n-type wafer, showing $S = 10\,600$ cm/s, but only a lower bound $\tau_b \geq 2$ ms bulk lifetime value can be given.

examples that although the spectral dependence of the data can be explained through the use of this model, it will not always be possible to separate the bulk from the contact effects.

Figure 9 shows the data obtained from the passivated and unpassivated HIT wafers and the model fit to the data. The results are plotted on log-linear axes for better comparison. Strong spectral dependence is observed for the unpassivated wafer, whereas the passivated wafer shows no significant dependence, indicating a low surface recombination velocity. The results of the model fit to the unpassivated wafer data reveals $S_{unpass} = 33\,300$ cm/s, but once again only a minimum value of $\tau_b \geq 1$ ms can be confidently stated. As for the surface recombination velocity of the passivated wafer, an upward bound value of $S_{pass} \leq 13.5$ cm/s can be given by setting $\tau_b \rightarrow \infty$, and fitting the model to the passivated wafer data. However, considering the minimum value of $\tau_b = 1$ ms, we can estimate a lower bound $S_{pass} \geq 5.7$ cm/s from the model fit to the data. This lower bound value for bulk lifetimes and the estimated passivated surface recombination

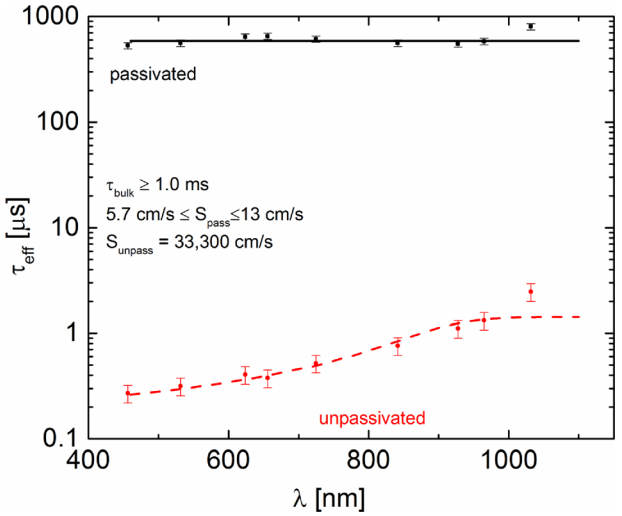

FIG. 9. Measured data and analytical model fit for an unpassivated and passivated n-type HIT wafer from the same batch. The model fit to the data gives a lower bound bulk lifetime estimate of $\tau_b \geq 1.0$ ms for both wafers, a range of passivated surface recombination velocities for the passivated wafer, $5.7 \leq S_{pass} \leq 13$ cm/s and $S_{unpass} = 33\,300$ cm/s. $D = 18\ cm^2/s$ was used for these calculations.

velocity range are consistent with other reports[39–41] for n-type HIT silicon.

Figure 10 shows the same type of data and modeling results from the PERC p-type wafers. In this case, the unpassivated effective lifetimes are below 100 ns (very low signals) and therefore the signal-to-noise ratio is low; nonetheless, a clear increasing τ_{eff} vs. λ trend can be observed. The analysis indicates that the bulk lifetimes for these wafers are at least $150\ \mu s$, with $235 \leq S_{pass} \leq 290$ cm/s and $S_{unpass} = 402\,000$ cm/s Just as the previous case, the results and the modeling clearly indicates a marked improvement in the effective lifetimes after the deposition of the emitter/passivation layers.

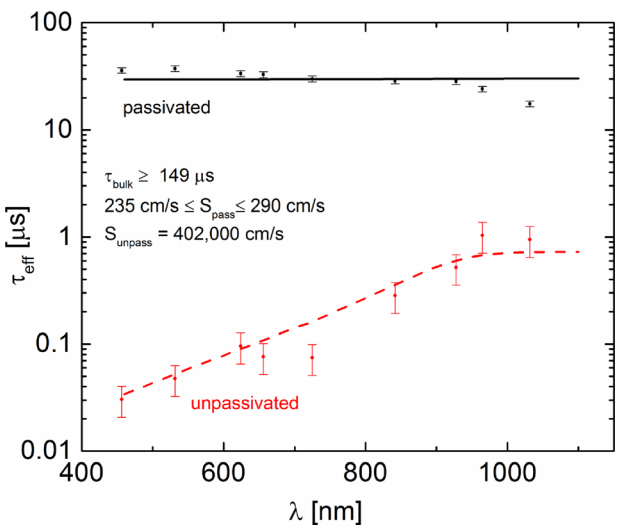

FIG. 10. Measured data and the analytical model fit for an unpassivated and passivated p-type PERC wafer from the same batch. Here, we can give a lower bound bulk lifetime estimate of $\tau_b \geq 0.15$ ms for both wafers, a range of passivated surface recombination velocities for the passivated wafer, $235 \leq S_{pass} \leq 290$ cm/s and $S_{unpass} = 402\,000$ cm/s, $D = 36\ cm^2/s$ for electrons were used for this p-type wafer.

E. Further discussion

The measurement results presented here show that the spectral dependent effects can be used to obtain meaningful information regarding the quality of the bulk material and the effects of surface treatments. The spectral dependent behavior of τ_{eff} can be explained very well with the analytical model of Eq. (12). However, care must be taken when reporting the physical parameters that are obtained from modeling the experimental results. Assuming a good accuracy regarding the experimental data, one can see that the model sensitivity is most limited when dealing with very thin wafers or cases of overwhelming dominance by surface recombination over bulk properties. In such cases, only a lower bound value can be given for bulk lifetimes. In the case of the high quality 1 mm thick wafer described earlier, one indeed finds, from the fit of model to the data, that $\tau_b \geq 2$ ms because the model will not fit to all the data well if τ_b was lower. However, nothing can be said about an upward bound. To see how high τ_b can be, we did some additional spectral dependent measurements on a thicker wafer slice of the same material. The equation predicts that the model sensitivity is substantially enhanced for thicker wafers. In fact, we did find that for this thicker 5 mm cut, the minimum τ_b would now have to be 30 ms, still not fully converging. This exercise demonstrates that certain limitations of the model can be overcome. On the other hand, when within the sensitivity range, such as the 550 μm n-type wafer of Fig. 8(a), both τ_b and S converge over the measurement results, and both parameters can be calculated with good confidence from just the one wafer measurement.

Regarding the high quality HIT and PERC wafers, we run into a situation where only a lower bound estimate can be given for the bulk lifetimes. In this case, the surface recombination velocities of the passivated wafers cannot be accurately given because to do so would require the precise knowledge of τ_b. If the manufacturers were able to provide a few varieties of thicker wafers, it may have been possible to converge on τ_b and use it on the passivated wafers to determine S_{pass}. In non-convergent cases, we can still estimate S_{pass} over a relatively tight region by considering the lower bound for τ_b and an upward bound of ∞ and see what S range would have to be in order to fit the passivated wafer data (which are constant, with insignificant λ dependence).

Regardless of whether the model is sensitive enough to separate bulk lifetimes and surface recombination velocities for a given wafer, the spectral dependent measurements of the effective lifetimes can be used as a tool to identify and characterize poor passivation. Figure 7 demonstrates the behavior that is expected of the spectral dependent measurements as a function of the surface recombination velocity. One interesting observation is that at the mid-range of S values, i.e., $10^3 - 10^4$ cm/s, the effective lifetime is relatively constant with λ in the range of 400 nm–800 nm, followed by a rise in the 800 nm–1100 nm range. Therefore, not a significant number of wavelength measurements are required in order to have confidence on model-fitted S values. However, for $S \sim 10^5$ cm/s or larger, a nonlinear relationship is observed between τ_{eff} and the wavelength; therefore more wavelength dependent measurements over the entire range will help in obtaining the best fit of the model to the data.

Although not presented here, the measurements of spectral lifetimes can also be performed as a function of the excess carrier density, to help obtain information regarding the various recombination phenomena such as the Shockley-Read-Hall (SRH) or emitter recombination. The measurements presented here were carried out with illumination intensities at or below 1 sun intensity, typically associated with the SRH regime in silicon. Exploring the spectral effects at higher intensity levels, possibly by using more powerful LEDs or other light sources, can provide more insight into the physics of charge carrier phenomena in these materials.

F. Pathlength enhancement

Due to the non-planar morphology of some of the wafers tested, the incident light on the sample will refract and transmit through the sample at a non-normal angle, thus increasing the length of its path through the wafer. This effect can result in a larger generation rate within the material than predicted by Equation (3), hence affecting the calculated lifetime. While this phenomenon is not an important issue for thick samples or irradiation by visible to NIR light LEDs where most photons are absorbed within a distance of their thickness, thin samples illuminated near the material's bandgap energy require a correction. In addition to a requirement for the distance of the first pass of the light to be altered based on the refraction angle, the reflection off the back surface of the wafer also needs to be considered. In thin samples, the longer wavelength LEDs will provide enough light transmission through the entirety of the wafer such that the backside reflections become significant.[30]

A detailed treatment of these optical effects is beyond the scope of this work. However, a convenient online tool from PV Lighthouse,[42] a wafer ray tracer, was used in order to calculate the estimates of effective pathlength enhancement factors based on the surface morphologies of the wafers and their thicknesses. This effective pathlength enhancement gave a factor that accounts for the enhanced photon absorption and charge generation within the wafer. This factor is multiplied by the width of the wafer to give an effective width at which the light travels within the material. This change is used in the calculations by altering the bounds on the integration for the generation rate. The pathlength enhancement factor was only relevant for the LED wavelengths greater than 900 nm, with estimated enhancement factors of 1.7 for the 965 nm LED and 16 for the 1032 nm LED.

V. CONCLUSIONS

The measurement apparatus developed for these experiments allowed for charge carrier excitation with a narrow spectral bandwidth source of illumination. Using this apparatus, spectral dependent charge carrier lifetime measurements were performed on a variety of silicon wafers, some from PV manufacturing plants during the various stages of the production. Spectral dependence of lifetimes appears in cases of high surface recombination velocity corresponding

to poorly or unpassivated wafers. The utility of a recently-developed analytical model to explain the spectral dependence of the lifetime data was investigated, and good agreements between the model and the experimental data were observed. Depending on the wafer thickness or the interplay between the bulk and the surface recombination effects, it may be possible to extract both bulk lifetimes and surface recombination velocities. However, in cases of high bulk lifetimes and domination of surface effects, the model fails to converge over a unique bulk lifetime and hence only a lower bound value can be obtained.

Although the light flux provided by the utilized LEDs was not as intense as the other input sources, a good measurement of the lifetime was attainable through averaging on a periodic input signal. The LEDs, when paired with the coupled light guide, were also able to provide a good uniformly lit area required by the coil measurement. Since this measurement is an aggregate measurement of the properties of a wafer, the specific carrier densities cannot be measured as a function of depth into the wafer. However, this depth dependence can be modeled using the diffusion equation and boundary conditions shown. The strength of the RF coil measurement lies in the measurement being done under quasi-steady state conditions, with monochromatic light intensities below 1 sun which are most similar to the conditions that a finished PV cell would encounter outdoors. Because the developed system was able to measure the carrier lifetimes down to the 30 ns range, this technique may be further used to measure other photovoltaic materials such as gallium arsenide and other III-V materials.

ACKNOWLEDGMENTS

B. H. Hamadani would like to thank Dr. Howard Yoon, Brian Dougherty, and Dr. William Healy for support and useful discussions throughout this work.

Y.-T. Li would like to thank Evan Chen and Rex Wang (Gintech Energy Company) and John Liu (Archers System) for their support and discussions during this work.

NIST disclaimer: Any mention of commercial products or reference to commercial organizations is for information only; it does not imply recommendation or endorsement by NIST nor does it imply that the products mentioned are necessarily the best available for that purpose.

[1]D. Klein, F. Wuensch, and M. Kunst, Phys. Status Solidi **245**, 1865 (2008).
[2]D. K. Schröder, IEEE Trans. Electron Devices **44**, 160 (1997).
[3]O. Palais and A. Arcari, J. Appl. Phys. **93**, 4686 (2003).
[4]Y.-I. Ogita, J. Appl. Phys. **79**, 6954 (1996).
[5]G. S. Kousik, Z. G. Ling, and P. K. Ajmera, J. Appl. Phys. **72**, 141 (1992).
[6]W. M. Bullis and H. R. Huff, J. Electrochem. Soc. **143**, 1399 (1996).
[7]A. G. Aberle, Prog. Photovoltaics Res. Appl. **8**, 473 (2000).
[8]R. A. Sinton, NREL Annual Subcontract Report No. NREL/SR-520-35884 (2004).
[9]K. Bothe, R. Krain, R. Falster, and R. Sinton, Prog. Photovoltaics Res. Appl. **18**, 204 (2010).
[10]M. Turek, J. Appl. Phys. **111**, 123703 (2012).
[11]M. Bail and R. Brendel, in Proceedings of the 16th European Photovoltaic Solar Energy Conference (2000), p. 1.
[12]J. Brody and A. Rohatgi, Solid State Electron. **46**, 859 (2002).
[13]T. Otaredian, Solid State Electron. **36**, 153 (1993).
[14]R. A. Sinton, in Proceedings of the 3rd World Conference on Photovoltaic Energy Conversion (2003), Vol. 1, p. 951.
[15]H. Mäckel and A. Cuevas, in Proceedings of the 3rd World Conference on Photovoltaic Energy Conversion (2003), p. 71.
[16]R. K. Ahrenkiel and S. W. Johnston, Sol. Energy Mater. Sol. Cells **93**, 645 (2009).
[17]L. Sirleto, A. Irace, G. Vitale, L. Zeni, and A. Cutolo, J. Appl. Phys. **93**, 3407 (2003).
[18]R. K. Ahrenkiel and J. Dashdorj, J. Vac. Sci. Technol. B **22**, 2063 (2004).
[19]R. K. Ahrenkiel and S. W. Johnston, Mater. Sci. Eng. B **102**, 161 (2003).
[20]J. Linnros, J. Appl. Phys. **84**, 275 (1998).
[21]R. A. Sinton and A. Cuevas, Appl. Phys. Lett. **69**, 2510 (1996).
[22]H. Nagel, C. Berge, and A. G. Aberle, J. Appl. Phys. **86**, 6218 (1999).
[23]Y. Arafat, F. M. Mohammedy, and M. M. Shahidul Hassan, Int. J. Optoelectron. Eng. **2**, 5 (2012).
[24]Z. G. Ling and P. K. Ajmera, J. Appl. Phys. **69**, 519 (1991).
[25]T. Pisarkiewicz, Opto-Electron. Rev. **12**, 33 (2004).
[26]R. J. Kumar, J. M. Borrego, R. J. Gutmann, J. R. Jenny, D. P. Malta, H. M. Hobgood, and C. H. Carter, J. Appl. Phys. **102**, 013704 (2007).
[27]F. Machuca, D. House, D. Cornwell, and P. Shaw, in Proceedings of the 26th EU PVSEC (2011), p. 1847.
[28]A. Cuevas and R. A. Sinton, Prog. Photovoltaics Res. Appl. **5**, 79 (1997).
[29]S. M. Sze and K. K. Ng, *Physics of Semiconductor Devices*, 3rd ed. (John Wiley and Sons, Inc., 2007).
[30]L. Zeng, Y. Yi, C. Hong, J. Liu, N. Feng, X. Duan, L. C. Kimerling, and B. A. Alamariu, Appl. Phys. Lett. **89**, 111111 (2006).
[31]D. Macdonald, M. Kerr, and A. Cuevas, Appl. Phys. Lett. **75**, 1571 (1999).
[32]D. Macdonald, R. A. Sinton, and A. Cuevas, J. Appl. Phys. **89**, 2772 (2001).
[33]R. K. Ahrenkiel and S. Johnston, Sol. Energy Mater. Sol. Cells **55**, 59 (1998).
[34]R. A. Bardos, T. Trupke, M. C. Schubert, and T. Roth, Appl. Phys. Lett. **88**, 053504 (2006).
[35]S. Bowden and R. A. Sinton, J. Appl. Phys. **102**, 124501 (2007).
[36]R. A. Sinton, T. Mankad, S. Bowden, and N. Enjalbert, in Proceedings of the 19th European Photovoltaic Solar Energy Conference (Paris, 2004), p. 520.
[37]M. Turek, C. Möller, and K. Lauer, in Proceedings of the 27th European Photovoltaic Solar Energy Conference and Exhibition (2012), p. 1045.
[38]A. Richter, S. W. Glunz, F. Werner, J. Schmidt, and A. Cuevas, Phys. Rev. B **86**, 165202 (2012).
[39]B. Stegemann, J. Kegel, M. Mews, E. Conrad, L. Korte, U. Sturzebecher, and H. Angermann, Energy Proc. **55**, 219 (2014).
[40]A. Goodrich, P. Hacke, Q. Wang, B. Sopori, R. Margolis, T. L. James, and M. Woodhouse, Sol. Energy Mater. Sol. Cells **114**, 110 (2013).
[41]S. Dauwe, J. Schmidt, and R. Hezel, in Proceedings of the 29th IEEE Photovoltaic Specialists Conference (New Orleans, 2002), p. 1246.
[42]See www.pvlighthouse.com.au/ for PV Lighthouse.